1

A Pod-Based Dual-Beam SAR

Gordon Farquharson, William N. Junek, Arun Ramanathan, Stephen J. Frasier, Russell Tessier, David J. McLaughlin, Mark A. Sletten, Jakov V. Toporkov

This work was supported by grants from the Office of Naval Research (Remote Sensing, N00014-98-1-0612), the Defense University Research Instrumentation Program (DURIP), the Air Force Office of Scientific Research, and by the Naval Research Laboratory (”Physics of INSAR-Based Ocean Surface Current Measurent”, WU# 72-8027)

Abstract

A dual-beam along-track interferometric synthetic aperture radar which is entirely self-contained within an aircraft pod has been developed by the University of Massachusetts to study sea surface processes in coastal regions. The radar operates at 5.3 GHz with a bandwidth of up to 25 MHz. System hardware is described. Initial test flights aboard the NOAA WP-3D research aircraft were performed to evaluate system performance over land and water surfaces. Imagery were collected for fore and aft squinted beams, though no interferometric data were collected. Notable look-angle dependences are observed in the sea surface NRCS under very low wind conditions.

Keywords

SAR, interferometry, sea surface scattering

I. INTRODUCTION

Synthetic aperture radar has long been a tool for remote sensing of the ocean surface. In the late 1980s, along-track interferometry (ATI) was implemented with synthetic aperture radar [1] and has since been applied to numerous sea surface wave and current studies [2], [3], [4], [5]. Along-track interferometry employs two radar antennas separated in the along track direction to obtain the line-of-sight (Doppler) component of the velocity of scatterers within the radar beam. By correlating the measurements of the two antennas at the appropriate temporal lag, two samples of the surface echo displaced in time are available. An extensive review of SAR interferometry discussing both cross-track and along-track techniques is given in [6].

A logical extension of along-track interferometry is to employ two squinted beams to obtain two components of velocity [7], [8]. The Dual-Beam Interferometer (DBI) described in this letter is a C-band SAR designed to enable estimates of the ocean surface current vector with a single pass of an aircraft. All radar electronics and data acquisition are contained within a wing-mounted pod. The pod represents a convenient and economical platform for airborne remote sensing.

In this letter we describe the radar instrument hardware and the airborne pod interface. We present dual-look SAR imagery over both land and water features obtained during initial engineering test flights. The following sections describe respectively the instrument hardware, engineering test flight conditions, and sample imagery obtained.

II. System Description

A photograph of the DBI radar system is shown in figure 1. In its present configuration, it consists of two pairs of squinted antennas which form two squinted interferometers, a pulse-compression radar transceiver, a data acquisition and control system, and a velocity/attitude measurement system.

Each interferometer consists of a pair of C-band microstrip patch array antennas separated by a baseline of 1.1 m. The antennas are designated by location (fore or aft) and orientation (fore or aft). Thus FF is the forward-located, forward-squinted antenna; FA is the foreward-located, aft-squinted antenna, and so on (see Fig 1). Antennas FF and AF comprise the forward looking interferometer while antennas AF and AA comprise the aft-looking interferometer. The forward located antennas are transmit-receive while the aft antennas receives only. As a result, the effective along-track baseline is half the physical baseline. The antennas are vertically polarized with half-power beamwidths of 7° (H-plane) and 31° (E-plane). The antennas are oriented with boresight towards 70° incidence and 20° squint angles. This orientation was chosen to provide gain at large incidence angles, though it may be adjusted.

A block diagram of the transceiver is shown in figure 2. Within the transmitter, a linear frequency-modulated chirp waveform is generated by a direct digital synthesizer, upconverted to 5.3 GHz, and transmitted through one of the fore antennas. The bandwidth of the transmitted waveform is programmable up to 25 MHz realizing a range resolution as fine as 6 m. While the DDS operates with a clock frequency of only 125 MHz, a frequency alias of the generated waveform at 300 MHz center frequency is selected for upconversion. A solid-state power amplifier produces 70 W output power, though cable and duplexer losses limit transmitted power to approximately 40 W.

A pair of receivers connected to both fore and aft antennas demodulate the received signals using an intermediate frequency of 300 MHz. Each receiver produces in-phase and quadrature outputs for the data acquisition system. The radar is periodically switched between fore and aft looks in a “ping-pong” fashion, while an internal calibration loop permits periodic monitoring of the transmitted chirp signal.

The radar also integrates GPS/INS information into the data stream. Attitude/position information is provided by a Boeing CMIGITS-II, a digital quartz inertial measurement unit (DQI)

with a 5-channel, L1 Coarse/Acquisition (C/A) code GPS engine. The system also accepts differential GPS corrections provided by the U.S. Coast Guard network of 300 kHz beacons. A VLF beacon receiver is also included within the pod to enable real-time differential GPS.

Data acquisition is provided by a pair of custom boards developed at the University of Massachusetts [9]. These incorporate two 12-bit 65 MSPS analog to digital converters each followed by real-time coherent integration and dual IDE disk interfaces for data storage. Up to 16-pulse coherent integration is implemented for each look. The radar switches beams between coherent integration periods. The coherent integrator and disk interface are implemented using a pair of field programmable gate arrays (FPGAs), and the board is controlled by a microprocessor which can also access data in shared memory on the board. The board also includes serial and ethernet communication ports for real-time monitoring (Fig 3). The system currently supports sustained data rates to disk of 6 MB/s per receiver. With 320 GB of onboard storage, the system can acquire up to 14 hours of data between backups.

The entire radar system is housed within an instrument pod that is mounted to a fixed pylon located under the wing of the aircraft. The pod payload area is approximately 1.5 m in length and 60 cm in diameter, and it supports a load of up to 120 kg. The payload is rigidly attached to the upper section of the pod as shown in Figure 1 while the lower section serves as an aerodynamic radome consisting of a woven composite material (SpectraVue) with a nomex core.

The pod obtains 400 Hz power from the aircraft engines through the mating pylon. All other communications and control are performed via a 2.4 GHz wireless interface to the operator in the fuselage. An embedded PC running the Linux operating system serves as the interface between the pod instrumentation and the wireless link. Thus, only a laptop computer is required within the aircraft to control and monitor the instrument. This arrangement substantially simplifies the aircraft installation procedure and enables the rapid deployment of this instrument. The bandwidth limitations of the wireless link currently preclude a real-time onboard SAR processor, though such may be implemented in the future.

III. Initial Results

During Dec 2002, initial test flights aboard NOAA's WP-3D research aircraft were performed from the NOAA Aircraft Operations Center in Tampa, FL. The pod was mounted on the left wing of the aircraft inboard of the engines. Test flights were flown on 13 Dec 2002, and 17 Dec

2002. Although a few installation constraints precluded full system testing, data were collected for antennas FF and FA corresponding to foreward and aft looks from the foreward pair of antennas (inadequate ventilation during flight resulted in overheating within the pod causing the data system for the aft antenna to fail). A NACA vent has since been installed to provide adequate cooling during flight.

Figure 4 shows a transect across Charlotte Harbor, just south of Port Charlotte and WNW of Ft. Myers, FL. Both forward and aft beams are shown from the forward set of antennas. The swath width is approximately 7 km resolved with moderate resolution of 17 m in range. The swath corresponds to large incidence angles between $65°$ and $85°$. Light surface winds of approximately 3-4 m/s were reported during the flights. Given these low winds, flight altitude was chosen to be approximately 600 m to enable large incidence angle measurements and reasonable signal to noise ratio.

These images were focused using an adaptation of the extended chirp scaling algorithm [10] implemented by the Naval Research Laboratory. In these images, range and azimuth resolution are approximately matched at 15 m spatial resolution with 66 independent looks. As a result of the large number of looks, very little speckle is evident in the imagery. Each pixel has a radiometric uncertainty (normalized variance) of less than 0.1 dB. Worst case pulse-compression sidelobes in this imagery were below -26 dB.

Sinuous surface slick features are observable over much of the water surface within the bay. Such features are commonly observable under light wind conditions and are attributed to biological sources (see e.g. [11]). Where present, the surface film modifies the surface tension of the water, suppressing the Bragg-resonant capillary waves that are responsible for the microwave echo even at these large incidence angles for VV polarization. Thus, slicks appear as dark regions in the imagery and indicate locations of surface current convergence where the slick material accumulates. Under stronger wind forcing, slicks tend to be broken up by the mechanical action of larger gravity waves.

After equalizing range dependences of land surface echoes, we note a generally more uniform echo is observed in the forward look while a weaker and more range-dependent echo is evident in the aft look. Although the noise floor on the aft look is slightly higher, there is evidence of a wind direction signature in the sea surface echoes between the looks. The orientation of the fore

look is more aligned with the wind than the aft look, suggesting how wind direction information may also be extracted from the DBI instrument.

IV. Summary

In this letter we have described a newly constructed dual-beam SAR which operates within a wing-mounted aircraft pod. Initial test flights aboard NOAA's WP-3D research aircraft demonstrated the functionality of the system. The comparative ease by which the system may be installed on this and other aircraft make the pod-based airborne radar an attractive concept for coastal remote sensing applications.

Acknowledgment

The authors gratefully acknowledge the generous logistical and technical support of the NOAA Aircraft Operations Center in Tampa, FL and the comments of the anonymous reviewers.

REFERENCES

[1] R. M. Goldstein, T. P. Barnett, and H. A. Zebker, "Remote sensing of ocean currents," *Science*, vol. 246, pp. 1282–1285, 1989.

[2] M. Marom, L. Shemer, and E. B. Thornton, "Energy density directional spectra of a nearshore wave field measured by interferometric synthetic aperture radar," *J. Geophys. Res.*, vol. 96, no. C12, pp. 22 125–22 134, 1991.

[3] D. R. Thompson and J. R. Jensen, "Synthetic aperture radar interferometry applied to ship-generated internal waves in the 1989 loch linnhe experiment," *J. Geophys. Res.*, vol. 98, no. C6, pp. 10,259–10,269, 1993.

[4] H. C. Graber, D. R. Thompson, and R. E. Carande, "Ocean surface features and currents measured with synthetic aperture radar inteferometry and hf radar," *J. Geophys. Res.*, vol. 101, no. C11, pp. 25,813–25,832, 1996.

[5] G. O. Marmorino, D. R. T. amd H. C. Graber, and C. L. Trump, "Correlation of oceanographic signatures appearing in synthetic aperture radar and interferometric synthetic aperture radar imagery with in situ measurements," *J. Geophys. Res.*, vol. 102, no. C8, pp. 18,723–18,736, 1997.

[6] P. A. Rosen, S. Hensley, I. R. Joughin, F. K. Li, , S. N. Madsen, E. Rodriguez, and R. M. Goldstein, "Synthetic aperture radar interferometry," *Proc. IEEE*, vol. 88, no. 3, pp. 333–382, 2000.

[7] E. Rodriguez, D. Imel, and B. Houshmand, "Two-dimensional surface currents using vector along-track interferometry," in *PIERS'95 Proceedings*, Seattle, WA, 1995, p. 763.

[8] S. J. Frasier and A. J. Camps, "Dual-beam interferometry for ocean surface current vector mapping," *IEEE Trans. Geosci. Rem. Sensing*, vol. 39, no. 2, pp. 401–414, 2001.

[9] A. Ramanathan, "Acquisition of remote sensing data on a reconfigurable platform," Master's thesis, University of Massachusetts, Amherst, 2003.

[10] A. Moreira and Y. Huang, "Airborne sar processing of highly squinted data using a chirp scaling algorithm with integrated motion compensation," *IEEE Trans. Geosci. Rem. Sensing*, vol. 32, no. 5, pp. 1029–1040, 1994.

[11] G. O. Marmorino, D. R. Lyzenga, and J. A. C. Kaiser, "Comparison of airborne synthetic aperture radar imagery with in-situ surface-slope measurements across gulf stream slicks and a convergence front," *J. Geophys. Res.*, vol. 104, no. C1, pp. 1405–1422, 1999.

LIST OF FIGURES

TABLE I

DBI PARAMETERS

Parameter	Specification
Center Frequency	5.3 GHz
Polarization	VV
Bandwith	5-25 MHz
Pulse width	10 μs
Pulse repetition frequency	12 KHz
Transmitted power	40 W
Receiver noise figure	3 dB
Platform height	1000 m
Platform velocity	100 m/s
Antenna Baseline	1.1 m
Boresight incidence angle	$70°$
Squint angle	$20°$
Azimuth Beamwidth	$7°$
Elevation Beamwidth	$30°$

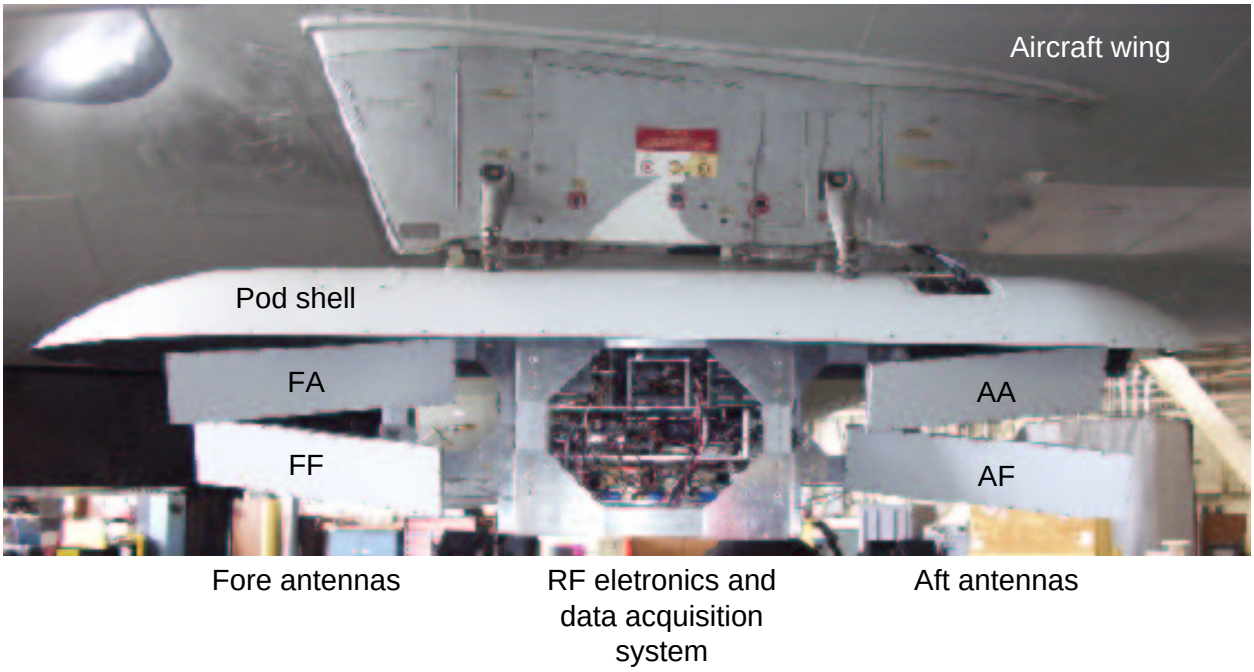

Fig. 1. Photo of DBI installed on P-3 wing pylon. The lower section of the pod is removed.

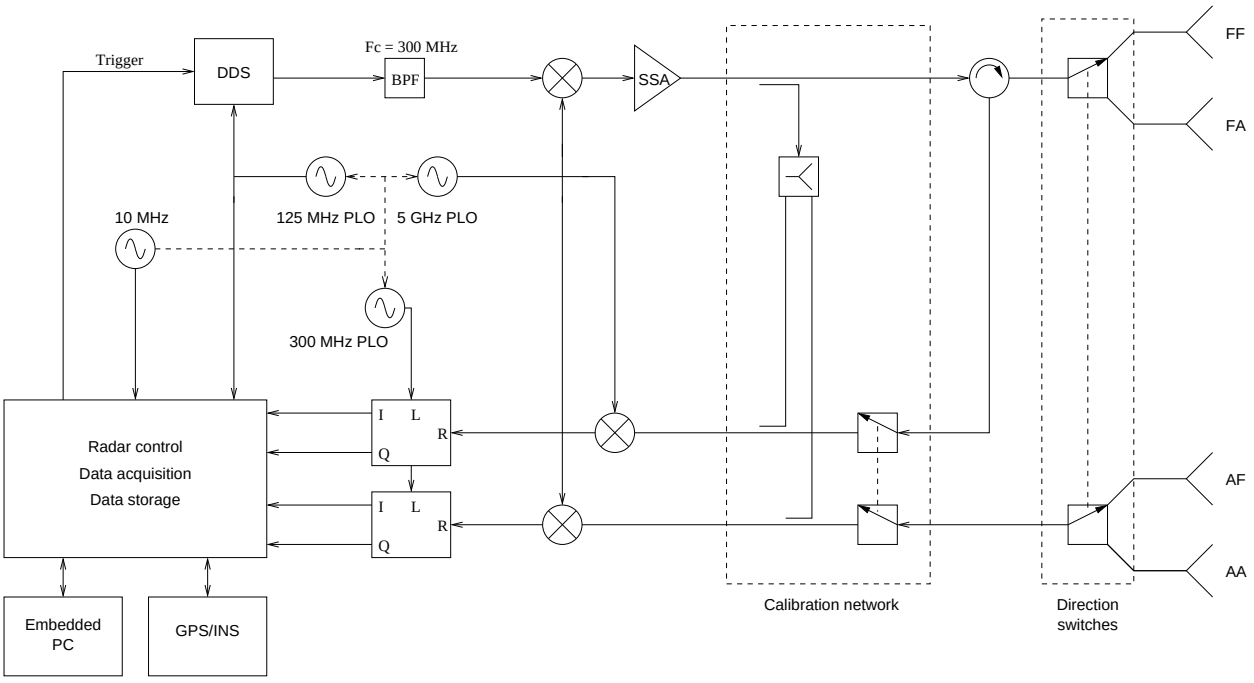

Fig. 2. Functional block diagram of DBI radar.

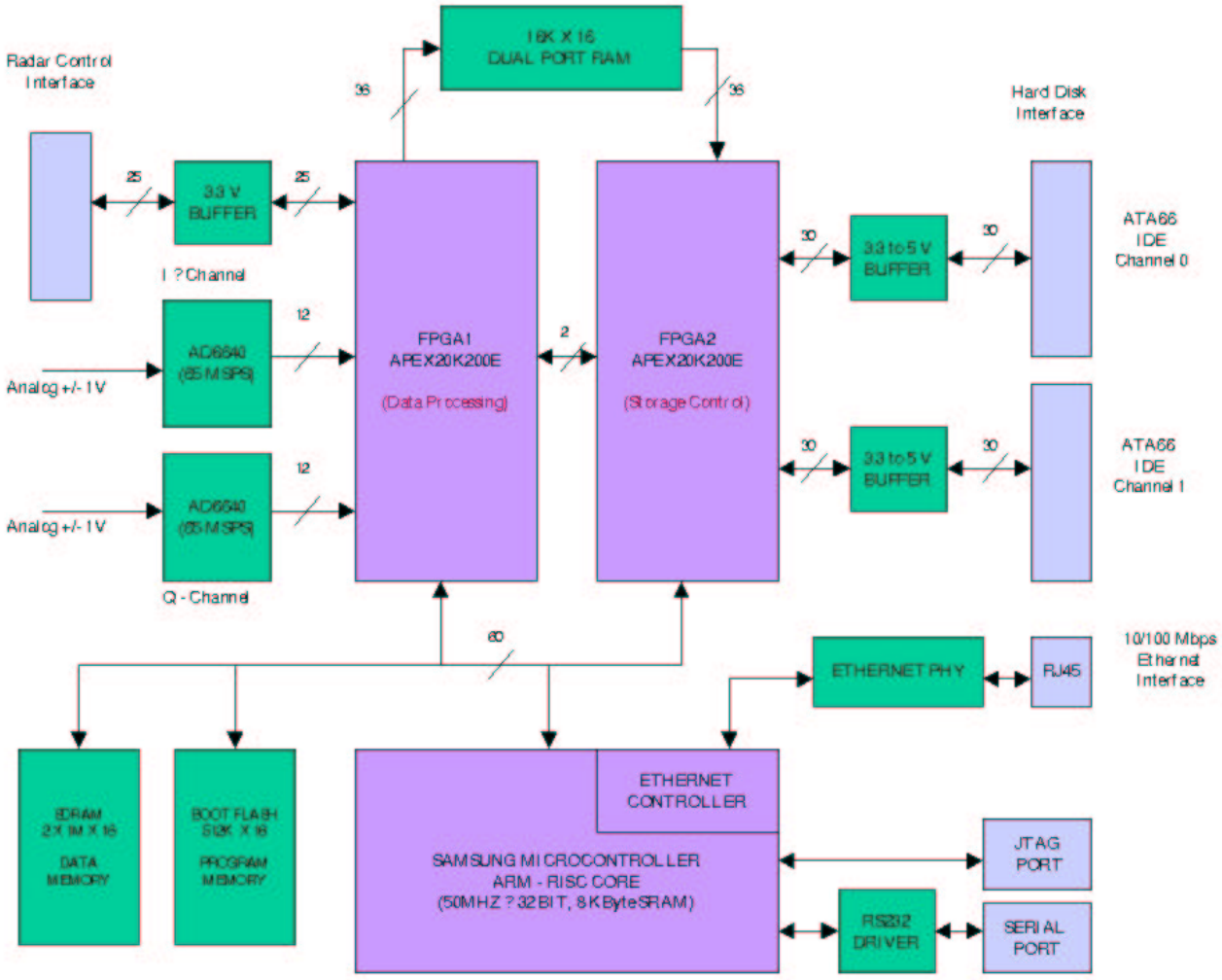

Fig. 3. Block diagram of FPGA-based data acquisition board developed at UMass: I and Q analog inputs at upper left, two Altera FPGAs and ARM microprocessor implement coherent integration and external interfaces, dual IDE disk interfaces on right.

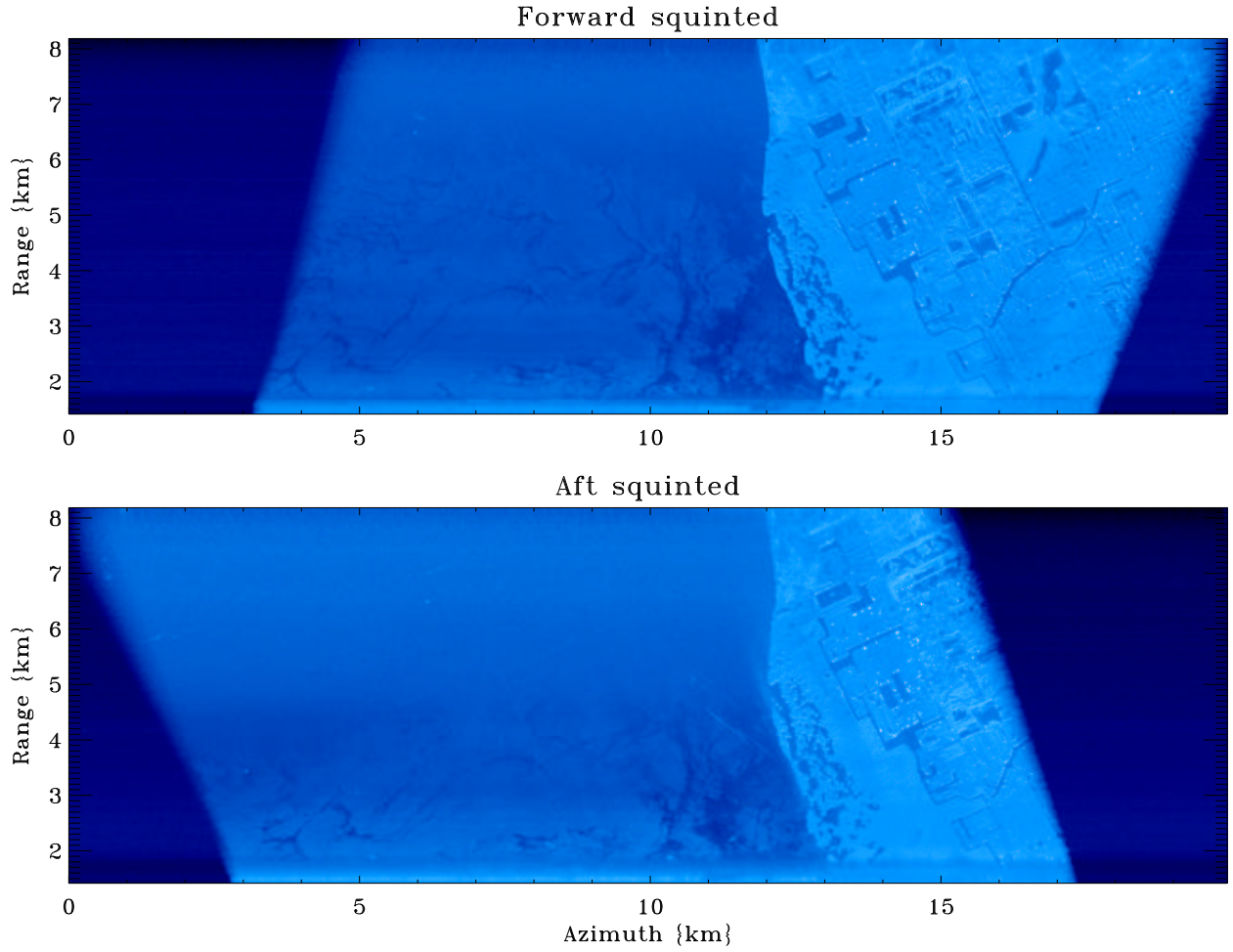

Fig. 4. Fore (top) and aft (bottom) views of surface slicks on Charlotte Harbor. An approximately 20 dB difference in NRCS exists between average land and sea surface echoes.